Electronic Supplementary Material (ESI) for ChemComm.

Electronic Supplementary Information

for

Ion-catalyzed synthesis of N/O co-doped carbon nanorods with hierarchical pores for high-rate Na-ion storage

Meixiang Cen,[a] Yingxue Cui,[a] Sherif A. El-Khodary,[a] Juan Wang,[a] Dickon H. L. Ng,[b] Shanhai Ge[c,]* and Jiabiao Lian[a,]*

[a] Institute for Energy Research, Jiangsu University, Zhenjiang 212013, P. R. China

[b] School of Science and Engineering, The Chinese University of Hong Kong (Shenzhen), Longgang, Shenzhen 518172, P. R. China

[c] Department of Mechanical Engineering, The Pennsylvania State University, University Park, PA 16802, USA

* Corresponding author: Tel/Fax: 0086-511-88799500.

E-mail: sug13@psu.edu (S. Ge.); jblian@ujs.edu.cn (J. Lian).

Experimental Section

Materials. Nitrilotriacetic acid (NTA) and manganese chloride ($MnCl_2$) were purchased from Macklin Chemical Reagent Co., Ltd (Shanghai, China). Isopropyl alcohol and hydrochloric acid (37 wt.%) were purchased from Sinopharm Chemical Reagent Co., Ltd (Shanghai, China).

Synthesis of the NOCNRs. Carbon nanorods were prepared by mixing 2.4 mg $MnCl_2$ and 1.8 mg NTA with 60 mL isopropyl alcohol. After stirring for 10 minutes, 20 mL deionized water was added to the above solution. After stirring for 30 minutes. The mixture was transferred to a Teflon-lined autoclave (100 mL) and kept at 180 ^oC for 6 hours. The precipitate (Mn-NTA) was collected by centrifugation and washing with ethanol 5 times, and then dried overnight at 60 ^oC in a vacuum oven. Subsequently, Mn-NTA was carbonized at 700 ^oC in H_2/Ar atmosphere (H_2/Ar=1/19 vol.) for 2 hours. The sample was etched with 2 M HCl overnight, and then washed to neutrality using deionized water. The sediment was transferred to a vacuum oven and dried at 60 °C for 12 hours. The final product was called N/O co-doped carbon nanorods (NOCNRs).

Characterizations. Morphology observations were performed on a field emission scanning electron microscope (FE-SEM, JEOL JSM-7800F), transmission electron microscopy (TEM, FEI Talos F200x G2) and high-resolution transmission electron microscope (HRTEM, super-X). The nitrogen adsorption–desorption measurements were conducted at 77 K using a Micromeritics Instrument Corporation (TriStar 3020). The phase and purity of the samples was confirmed by the powder X-ray

diffractometer (XRD, German Bruker D8 diffractometer, Cu Kα radiation (λ=1.5418 Å) and a scan rate of 7° min^{-1}). Raman spectrum was recorded on a Zolix RTS2 Confocal Laser Raman microscope at the excitation wavelength of 532 nm. The chemical structure of the product was characterized by Fourier transform infrared spectroscopy (FTIR, Thermo Scientific Nicolet iS20). The X-ray photoelectron spectrometer (XPS) was acquired on the Thermo Scientific K-Alpha X-ray photoelectron spectrometer, and the binding energy was calibrated using the C 1s peak at 284.8 eV as a reference.

Fabrication of Na metal half-cells. CR2032-type coin cells were assembled in an Ar filled glove box (H_2O and O_2 content < 0.1 ppm). The working electrode was prepared by coating *N*-methylpyridine (NMP) slurry containing active materials (70 wt.%), polyvinylidene fluoride (15 wt.%), and super-P carbon black (15 wt.%) on a copper foil current collector, followed by drying at 50 °C for 12 h in a vacuum oven. The mass loading of active material is 0.6–0.8 mg cm^{-2}. The electrochemical performance was tested utilizing CR2032 type coin cells with a sodium metal chip as counter and reference electrodes and 1 mol L^{-1} $NaPF_6$ in diglyme as electrolyte.

Electrochemical measurements. Galvanostatic intermittent titration technique (GITT) and galvanostatic charge–discharge (GCD) tests were collected on a LAND battery tester (CT2001A) at 25 °C. The galvanostatic intermittent titration technique (GITT) was carried out using current pulses (100 mA g^{-1}) with a duration of 10 min and a relaxation process over 1.0 h. Cyclic voltammetry (CV) and electrochemical impedance

spectroscopy (EIS, frequency range: 100 kHz–0.01 Hz) were recorded on the Gamry electrochemical workstation (Interface 1000E).

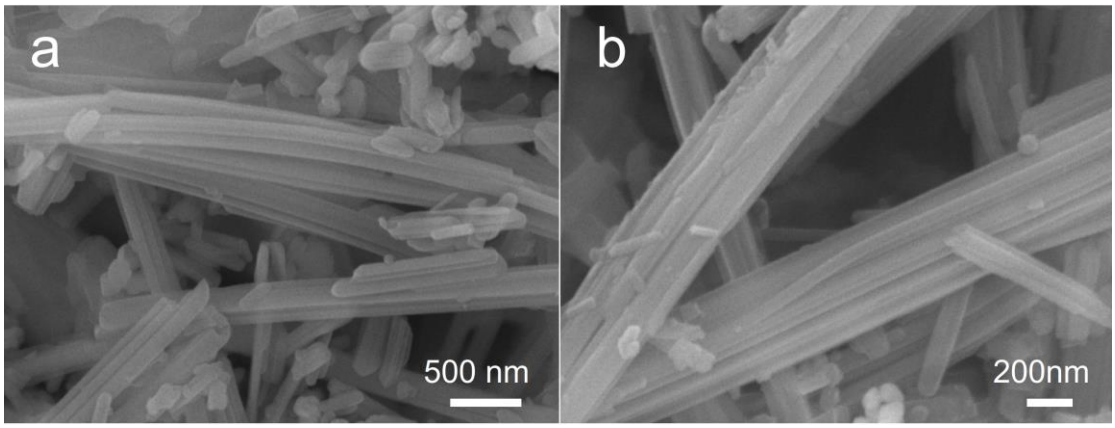

Fig. S1 (a, b) FE-SEM images of the Mn-NTA nanorods.

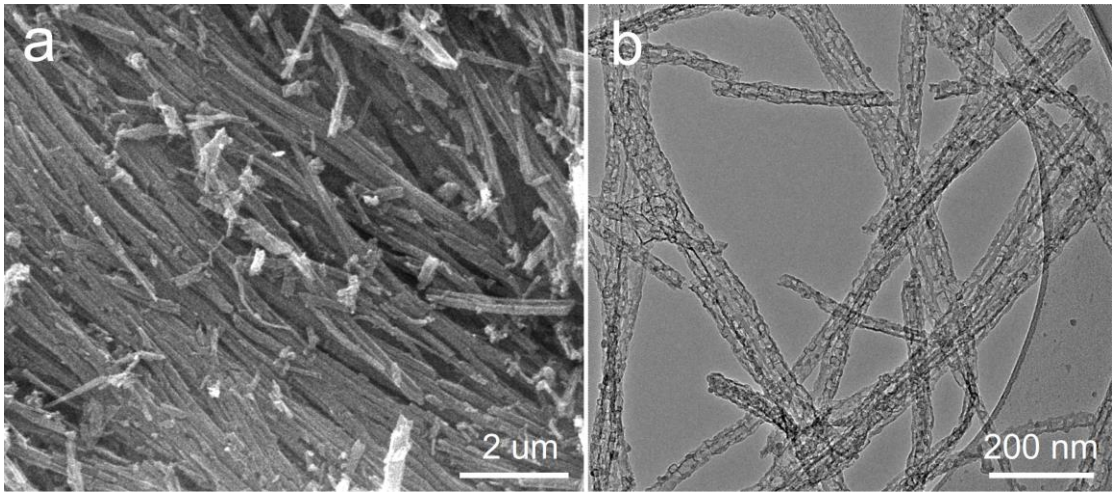

Fig. S2 (a) FE-SEM and (b) TEM images of the NOCNRs.

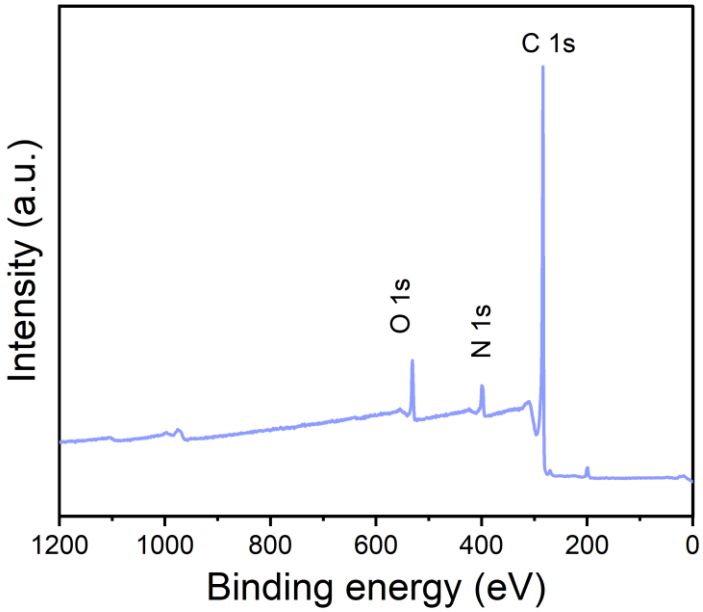

Fig. S3 XPS survey spectrum of the NOCNRs.

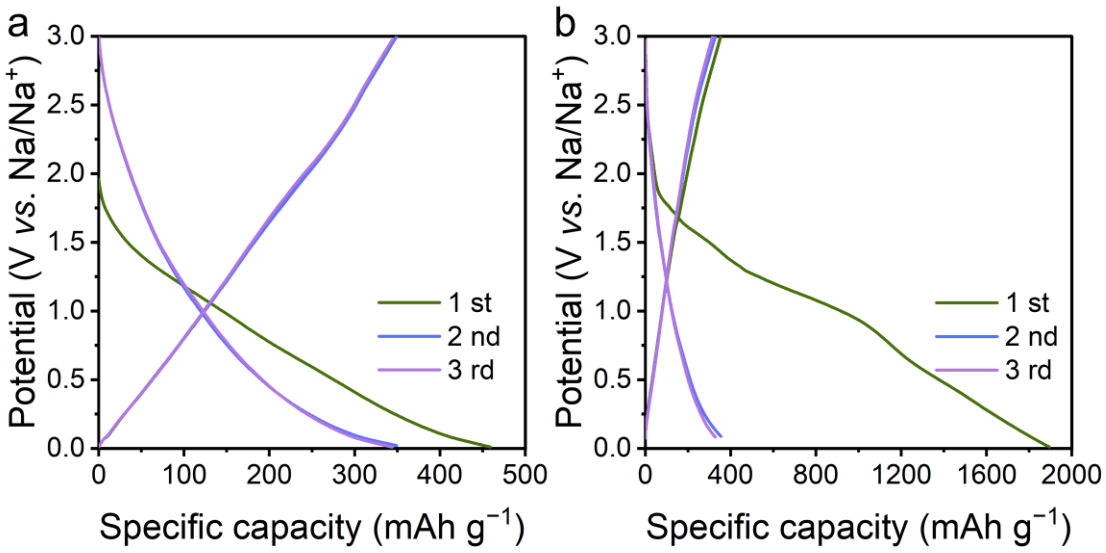

Fig. S4 GCD curves of the NOCNRs at 0.1 A g^{-1} in (a) ether-based (1.0 M $NaPF_6$ in diglyme) and (b) ester-based (1.0 M $NaClO_4$ in a mixture of ethylene carbonate and diethyl carbonate with a volume ratio of 1:1) electrolyte.

As shown in Fig. S4, hard carbon electrodes in the ether-based electrolyte can provide a higher initial Coulombic efficiency (ICE, 76.0%) compared with that in the ester-based electrolyte (18.6%), which is mainly due to the formation of a thin and stable solid electrolyte interface (SEI).[S1] Therefore, 1 mol L^{-1} $NaPF_6$ in diglyme was chosen as electrolyte in this work.

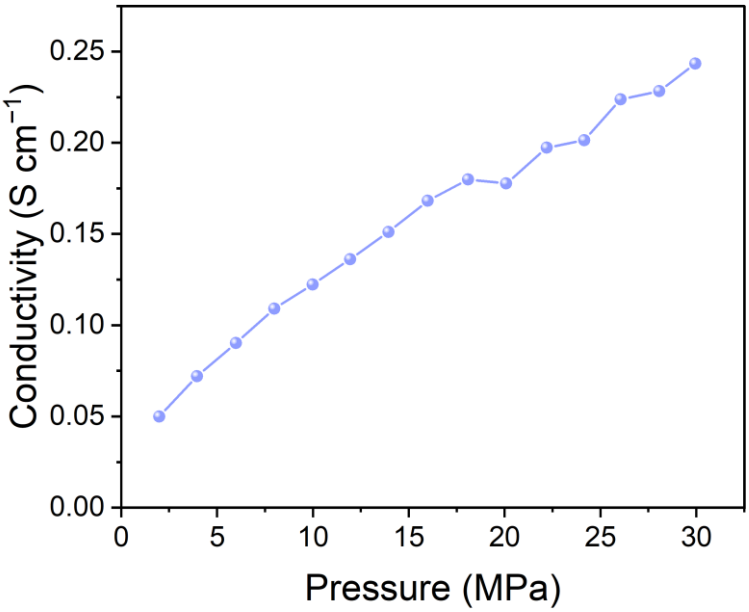

Fig. S5 Electronic conductivity of the NOCNRs.

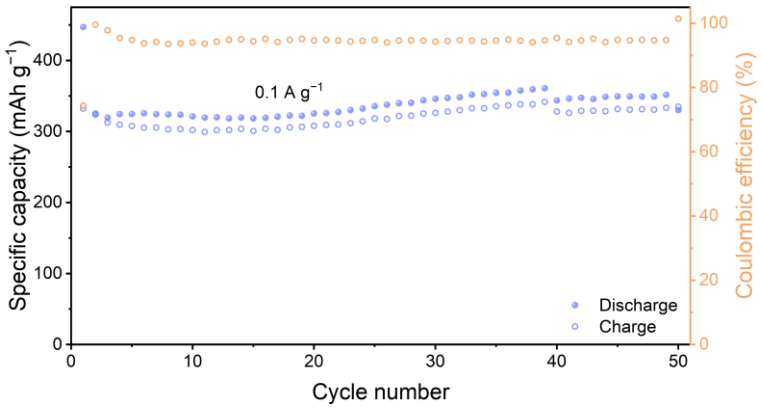

Fig. S6 Cycle performance of the NOCNRs electrode at a current density of 0.1 A g^{-1} within a potential window of 0.01–3.0 V.

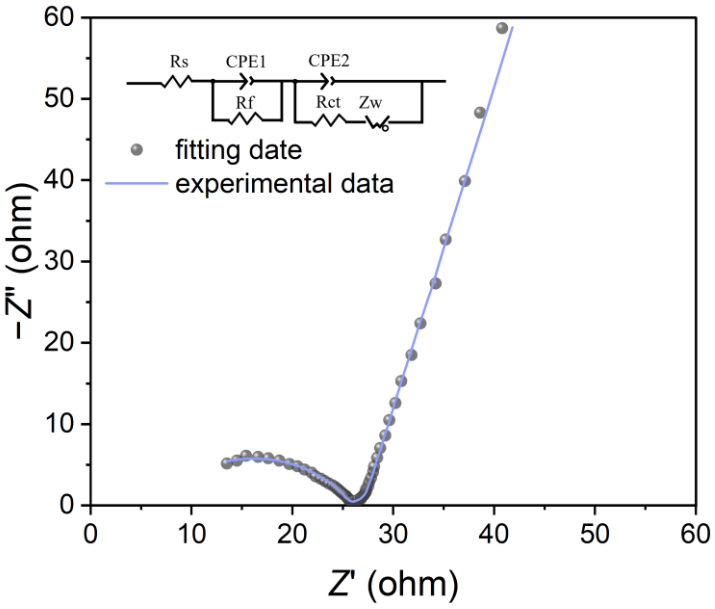

Fig. S7 Nyquist plot of the NOCNRs electrode after 100 cycles (inset: the corresponding equivalent circuit model).

Compared with the charge transfer resistance (R_{ct}) and equivalent series resistance (R_s) values before the cycle, the NOCNRs electrode shows a lower R_{ct} of 6.59 Ω and a smaller R_s of 6.58 Ω after 100 cycles within the potential window of 0.01–3.0 V, which can be ascribed to the component and morphology reconfigurable of solid electrolyte interphase (SEI) film.[S2]

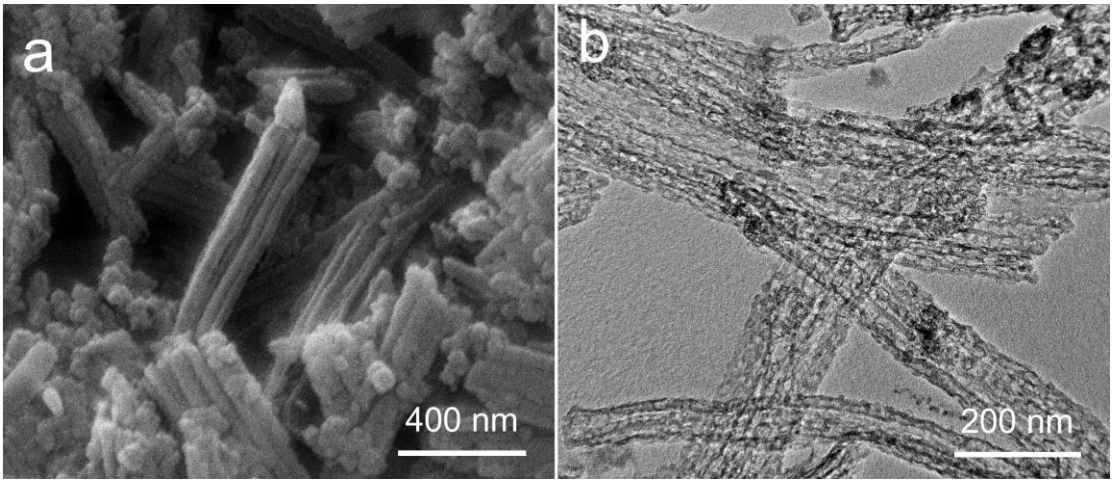

Fig. S8 (a) FE-SEM and (b) TEM images of the NOCNRs after 100 cycles at a current density of 10.0 A g^{-1}.

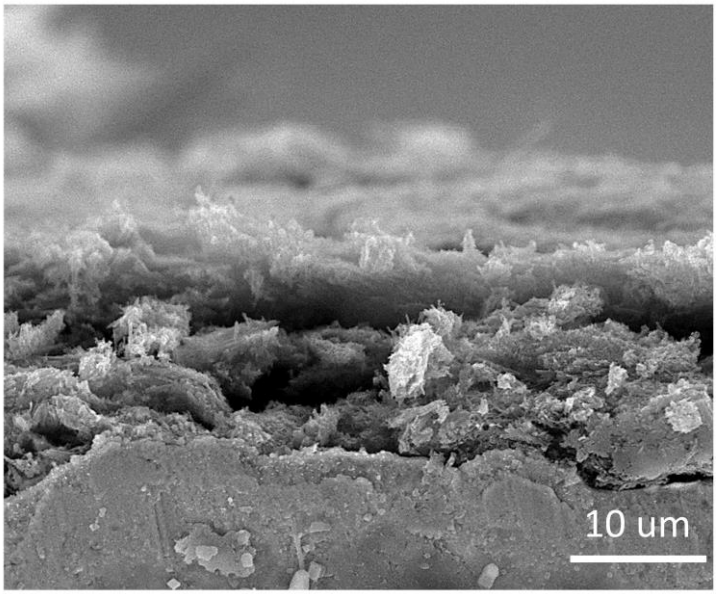

Fig. S9 Cross-section FE-SEM image of the NOCNRs electrode after cycling.

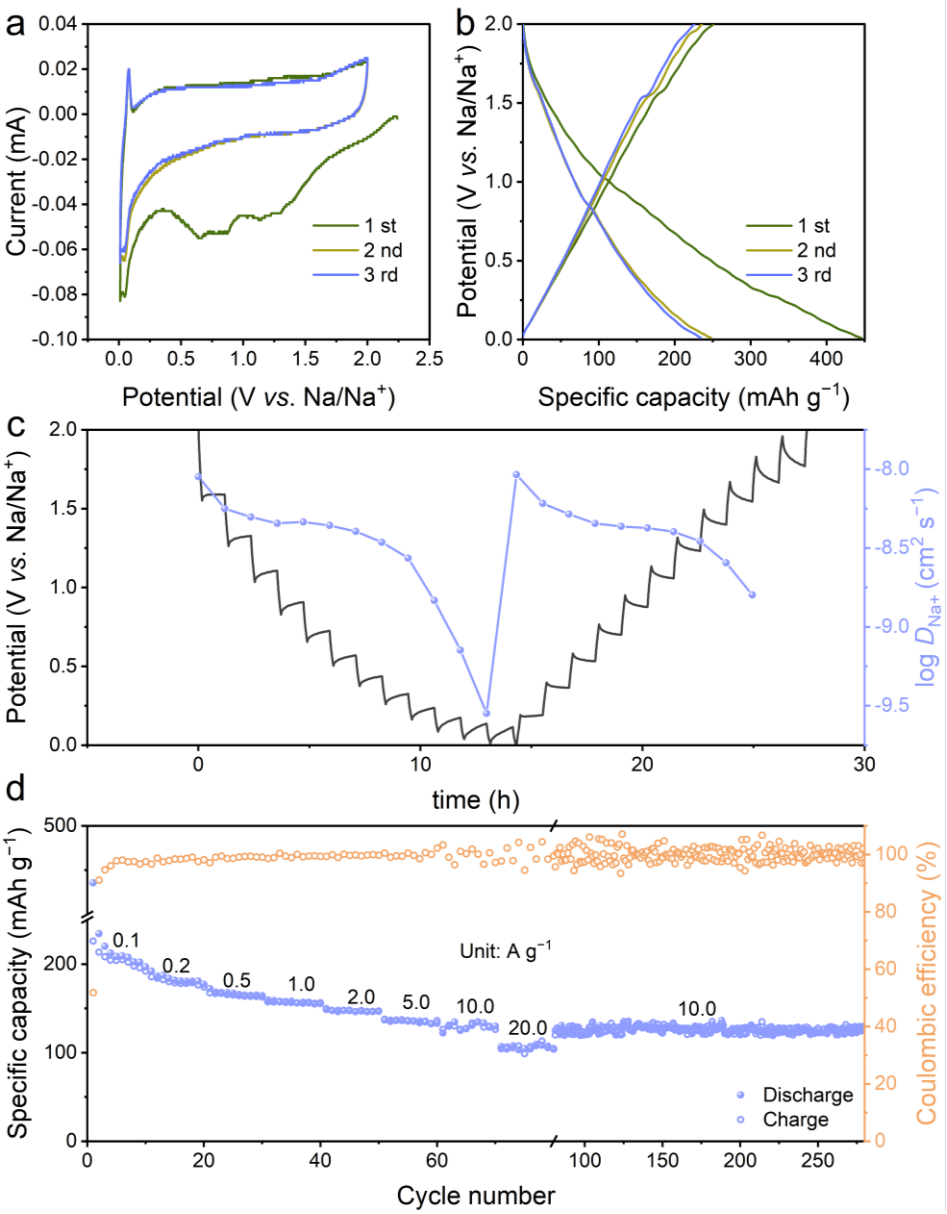

Fig. S10 Electrochemical performance of the NOCNRs electrode within the potential window of 0.01–2.0 V. (a) Initial three CV curves at 0.1 mV s^{-1}. (b) GCD curves at 0.1 A g^{-1}. (c) GITT profile with the calculated Na^+ diffusion coefficients (D_{Na+}). (d) Rate capability and cycling stability.

Figs. S10a† and S10b† show the CV curves at 0.1 mV s^{-1} and GCD profiles at 0.1 A g^{-1} in the initial three cycles of the NOCNRs within the potential window of 0.01–2.0

V, respectively. The initial Coulombic efficiency is 56.4%. The GITT results (Fig. S10c†) show that the D_{Na+} values to surface physical adsorption (1.5–2.0 V), surface functional groups (0.5–1.5 V), and graphite intercalation behavior (0.01–0.5 V) are 9.0×10^{-9}, 4.6×10^{-9} and 2.8×10^{-10} cm^2 s^{-1}, respectively. As shown in Fig. S10d†, the NOCNRs electrode exhibits rate capability of 205, 178, 164, 156, 146, 135, 127, and 107 mAh g^{-1} at current densities of 0.1, 0.2, 0.5, 1.0, 2.0, 5.0, 10.0, and 20.0 A g^{-1}, respectively. The capacity decay can reach 48% from 0.1 to 20.0 A g^{-1}. The cycling test of NOCNRs shows a capacity of 122 mAh g^{-1} at 10.0 A g^{-1} over 200 cycles (Fig. S10d†).

Table S1 The Electrochemical impedance fitting results of NOCNRs and other carbon electrodes.

Sample	R_s (ohm)	R_{ct} (ohm)	Z_w (ohm)	σ (ohm $s^{-1/2}$)
NOCNRs	**9.70**	**18.47**	**8.12**	**26.65**
N, S co-doped carbon[S3]	4.3	276.7	-	-
Esterified starch derived carbon[S4]	4.9	127	-	-
Old-loofah derived carbon[S5]	6.9	194.6	-	22.5
Xylose derived carbon[S6]	23.93	64.36	-	-
Sucrose derived carbon[S7]	11.22	118.7	-	-
Polyvinylpyrrolidone derived carbon[S8]	5.04	539	-	-
Poplar wood derived carbon[S9]	4.6	48.4	-	-
MXene-Bonded Flexible Hard Carbon[S10]	5.0	82	69	-
Pine pollen derived carbon[S11]	12.1	76.9	-	-
Borassus flabellifer derived carbon[S12]	9.41	46.7	-	-

Table S2 Electrochemical performance of NOCNRs and other carbon electrodes for sodium ion batteries.

Electrode	Electrolyte	Reversible specific capacity and rate capability	Cycling performance	ICE (%)
This work	**1 M $NaPF_6$ in diglyme**	**336 mAh g^{-1} at 0.1 A g^{-1} 196 mAh g^{-1} at 20.0 A g^{-1}**	**200 mA h g^{-1} at 10.0 A g^{-1} over 1300 cycles**	**76.0**
Commercial hard carbon[S13]	1 M $NaPF_6$ in THF	305 mAh g^{-1} at 0.02 A g^{-1} 212 mAh g^{-1} at 5.0 A g^{-1}	199 mA h g^{-1} at 5.0 A g^{-1} over 1000 cycles	
Rosewood derived carbon[S14]	1 M $NaPF_6$ in DME	326 mAh g^{-1} at 0.02 A g^{-1} 230 mAh g^{-1} at 5.0 A g^{-1}	250.9 mA h g^{-1} at 0.5 A g^{-1} over 800 cycles	71.2
Pine bulks derived carbon[S15]	1 M $NaPF_6$ in Diglyme	354.6 mA h g^{-1} at 0.03A g^{-1} 224.7 mA h g^{-1} at 2.0 A g^{-1}	243 mA h g^{-1} at 1.0 A g^{-1} over 5000 cycles	88.7
Chitosan derived carbon[S16]	1 M $NaPF_6$ in DME	267.5 mA h g^{-1} at 0.02A g^{-1} 139 mA h g^{-1} at 10.0 A g^{-1}	196 mA h g^{-1} at 1.0 A g^{-1} over 2000 cycles	85.9
Commercial hard carbon[S17]	1 M $NaClO_4$ in TEGDME	250 mA h g^{-1} at 0.05A g^{-1} 132 mA h g^{-1} at 1.0 A g^{-1}	196 mA h g^{-1} at 0.5 A g^{-1} over 1000 cycles	70.3
Loofah sponge derived carbon[S18]	1 M $NaCF_3SO_3$ in DEGDME	320 mA h g^{-1} at 0.03A g^{-1} 75 mA h g^{-1} at 6.0 A g^{-1}	178.7 mA h g^{-1} at 2.1 A g^{-1} over 2000 cycles	63
Sucrose derived hard carbon[S19]	0.8 M $NaPF_6$ in DEGDME	270 mA h g^{-1} at 0.02A g^{-1} 65 mA h g^{-1} at 5.0 A g^{-1}	200 mA h g^{-1} at 0.5 A g^{-1} over 1000 cycles	83.8
Tissue derived carbon[S20]	1 M NaOTf in Diglyme	338.2 mA h g^{-1} at 0.02A g^{-1} 170 mA h g^{-1} at 2.0 A g^{-1}	286.5 mA h g^{-1} at 0.2 A g^{-1} over 1000 cycles	91.2
Bacterial cellulose derived carbon[S21]	1 M $NaPF_6$ in DME	355 mA h g^{-1} at 0.1A g^{-1} 255 mA h g^{-1} at 10.0 A g^{-1}	310 mA h g^{-1} at 1.0 A g^{-1} over 1100 cycles	

THF: tetrahydrofuran, DME: 1,2-dimethoxy-ethan, TEGDME: tetraethylene glycol dimethyl ether, DEGDME: diethylene glycol dimethyl ether.

Supplementary References

S1 Y. Li, F. Wu, Y. Li, M. Liu, X. Feng, Y. Bai and C. Wu, *Chem. Soc. Rev.*, 2022, **51**, 4484–4536.

S2 Y. Huang, M. Xie, J. Zhang, Z. Wang, Y. Jiang, G. Xiao, S. Li, L. Li, F. Wu and R. Chen, *Nano Energy*, 2017, **39**, 273–283.

S3 Q. Jin, K. Wang, P. Feng, Z. Zhang, S. Cheng and K. Jiang, *Energy Storage Mater.*, 2020, **27**, 43–50.

S4 M. Song, Z. Yi, R. Xu, J. Chen, J. Cheng, Z. Wang, Q. Liu, Q. Guo, L. Xie and C. Chen, *Energy Storage Mater.*, 2022, **51**, 620–629.

S5 C. Yu, H. Hou, X. Liu, Y. Yao, Q. Liao, Z. Dai and D. Li, *Int. J. Hydrogen Energy*, 2018, **43**, 3253–3260.

S6 R. Dong, L. Zheng, Y. Bai, Q. Ni, Y. Li, F. Wu, H. Ren and C. Wu, *Adv. Mater.*, 2021, **33**, 2008810.

S7 L. Xiao, H. Lu, Y. Fang, M. L. Sushko, Y. Cao, X. Ai, H. Yang and J. Liu, *Adv. Energy Mater.*, 2018, **8**, 1703238.

S8 Y. Li, Y. Yuan, Y. Bai, Y. Liu, Z. Wang, L. Li, F. Wu, K. Amine, C. Wu and J. Lu, *Adv. Energy Mater.*, 2018, **8**, 1702781.

S9 Y. Zheng, Y. Lu, X. Qi, Y. Wang, L. Mu, Y. Li, Q. Ma, J. Li and Y.-S. Hu, *Energy Storage Mater.*, 2019, **18**, 269–279.

S10 N. Sun, Q. Zhu, B. Anasori, P. Zhang, H. Liu, Y. Gogotsi and B. Xu, *Adv. Funct. Mater.*, 2019, **29**, 1906282.

S11 Y. Zhang, X. Li, P. Dong, G. Wu, J. Xiao, X. Zeng, Y. Zhang and X. Sun, *ACS Appl. Mater. Interfaces*, 2018, **10**, 42796–42803.

S12 T. K. Kumaresan, S. A. Masilamani, K. Raman, S. Z. Karazhanov and R. Subashchandrabose, *Electrochim. Acta*, 2021, **368**, 137574.

S13 Z. Tang, H. Wang, P. F. Wu, S. Y. Zhou, Y. C. Huang, R. Zhang, D. Sun, Y. G. Tang and H. Y. Wang, *Angew. Chem., Int. Ed.*, 2022, **61**, e202200475.

S14 S. Zhou, Z. Tang, Z. Pan, Y. Huang, L. Zhao, X. Zhang, D. Sun, Y. Tang, A. S. Dhmees and H. Wang, *SusMat*, 2022, **2**, 357–367.

S15 W. Deng, Y. Cao, G. Yuan, G. Liu, X. Zhang and Y. Xia, *ACS Appl. Mater. Interfaces*, 2021, **13**, 47728–47739.

S16 Y. He, P. Bai, S. Gao and Y. Xu, *ACS Appl. Mater. Interfaces*, 2018, **10**, 41380–41388.

S17 B. Xiao, F. A. Soto, M. Gu, K. S. Han, J. Song, H. Wang, M. H. Engelhard, V. Murugesan, K. T. Mueller and D. Reed, *Adv. Energy Mater.*, 2018, **8**, 1801441.

S18 Y.-E. Zhu, L. Yang, X. Zhou, F. Li, J. Wei and Z. Zhou, *J. Mater. Chem. A*, 2017, **5**, 9528–9532.

S19 P. Bai, Y. He, P. Xiong, X. Zhao, K. Xu and Y. Xu, *Energy Storage Mater.*, 2018, **13**, 274–282.

S20 B.-H. Hou, Y.-Y. Wang, Q.-L. Ning, W.-H. Li, X.-T. Xi, X. Yang, H.-J. Liang, X. Feng and X.-L. Wu, *Adv. Mater.*, 2019, **31**, 1903125.

S21 Q. Jin, W. Li, K. Wang, P. Feng, H. Li, T. Gu, M. Zhou, W. Wang, S. Cheng and K. Jiang, *J. Mater. Chem. A*, 2019, **7**, 10239–10245.